ACS OMEGA

http://pubs.acs.org/journal/acsodf

Article

Improved Self-Assembly of P3HT with Pyrene-Functionalized Methacrylates

Taniya M. S. K. Pathiranage, Ziyuan Ma, Chinthaka M. Udamulle Gedara, Xiangcheng Pan, Youngmin Lee, Enrique D. Gomez, Michael C. Biewer, Krzysztof Matyjaszewski, and Mihaela C. Stefan*

Cite This: *ACS Omega* 2021, 6, 27325−27334

Read Online

ACCESS | Metrics & More | Article Recommendations | Supporting Information

ABSTRACT: A block copolymer with discotic liquid crystalline behavior was synthesized using Grignard metathesis polymerization (GRIM) and initiators for continuous activator regeneration atom transfer radical polymerization (ICAR-ATRP). A novel discotic liquid crystalline mesogen, 6-(pyren-1-yloxy)hexyl methacrylate (PyMA), comprises a block that is attached to regioregular poly(3-hexylthiophene) (*rr*-P3HT) generated by GRIM and subjected to end-group modification. Due to the continuous regeneration of Cu^{+} in the reaction mixture in ICAR-ATRP compared to conventional methods, the synthesis was successfully performed with less catalyst. The purity and yield of the final product are increased by eliminating rigorous post-synthesis purification. Stacked pyrene units have contributed to the enhanced long-range $\pi-\pi$ interactions and aligning of the P3HT block as observed in thin-film X-ray diffraction (XRD). Furthermore, field-effect mobilities in the order of 10^{-2} cm^2 V^{-1} s^{-1} in bottom-gate, top-contact organic field-effect transistors (OFETs) suggest an enhancement in charge transport due to the discotic electron-rich pyrene units that help mitigate the insulating effect of the methacrylate backbone. The formation of uniform microdomains of P3HT-*b*-poly(PyMA) observed with tapping mode atomic force microscopy (TMAFM) on the channel regions of OFETs indicates the unique packing of the block copolymer in comparison to pristine P3HT. Thermotropic properties of the novel discotic mesogen in the presence and absence of P3HT were observed with both the poly(3-hexylthiophene)-*b*-poly(6-(pyren-1-yloxy)hexyl methacrylate) (P3HT-*b*-poly(PyMA)) block copolymer and poly(6-(pyren-1-yloxy)hexyl methacrylate) (poly(PyMA)) homopolymer using polarized optical microscopy (POM) and differential scanning calorimetry (DSC).

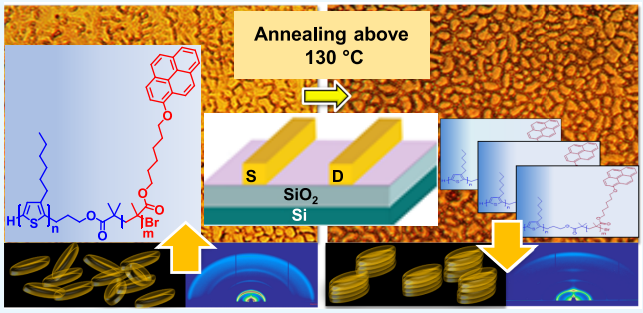

INTRODUCTION

A variety of studies have been carried out during the past few decades to improve organic semiconductors. Low manufacturing cost and the ability to make large area, flexible, and lightweight devices make organic semiconductors valuable materials. Studies based on different approaches have been reported on organic photovoltaics (OPVs),[1−3] organic field-effect transistors (OFETs),[4−6] organic light-emitting diodes (OLEDs),[7−9] organic lasers,[10,11] and memory devices.[12,13] For the fabrication of efficient organic electronic devices, tuning of the mechanical properties and charge transport of organic semiconductors has to be addressed through the development of structure−property relationships.[14,15] Organic semiconductors are highly versatile materials that can be functionalized to tune function, morphology, and optical properties. To that end, regioregular poly(3-hexylthiophene) (*rr*-P3HT) is among the extensively studied semiconducting polymers that have been tested as the active component in organic electronic applications.[16,17]

Many rod-coil block copolymers that consist of P3HT are reported to exhibit good optoelectronic properties. Rod-coil diblock and triblock copolymers with P3HT were synthesized using Grignard metathesis polymerization (GRIM) and other living polymerization techniques.[18−26] The synthesis of rod-rod block copolymers with P3HT was performed by attaching a liquid crystalline block to P3HT. There are a few recent reports based on the synthesis of all conjugated block copolymers based on P3HT or a block copolymer with liquid crystalline blocks attached to P3HT.[27,28] Stefan's group reported P3HT block copolymers comprising poly(γ-benzyl-L-glutamate) and poly(*N*-hexylisocyanate).[27,28] In another report, Lin and co-workers had demonstrated the synthesis of a P3HT-*b*-poly(3-butylthiophene) diblock copolymer with greatly improved crystallinity and electrical conductivity upon solvent annealing.[29] Apart from that, Peng et al. recently

Received: August 4, 2021
Accepted: September 8, 2021
Published: October 8, 2021

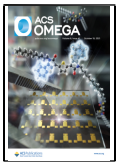

Scheme 1. Synthesis of Poly(3-hexylthiophene)-*b*-poly(6-(pyren-1-yloxy)hexyl methacrylate) (P3HT-*b*-poly(PyMA)) and Poly(6-(pyren-1-yloxy)hexyl methacrylate) (poly(PyMA))

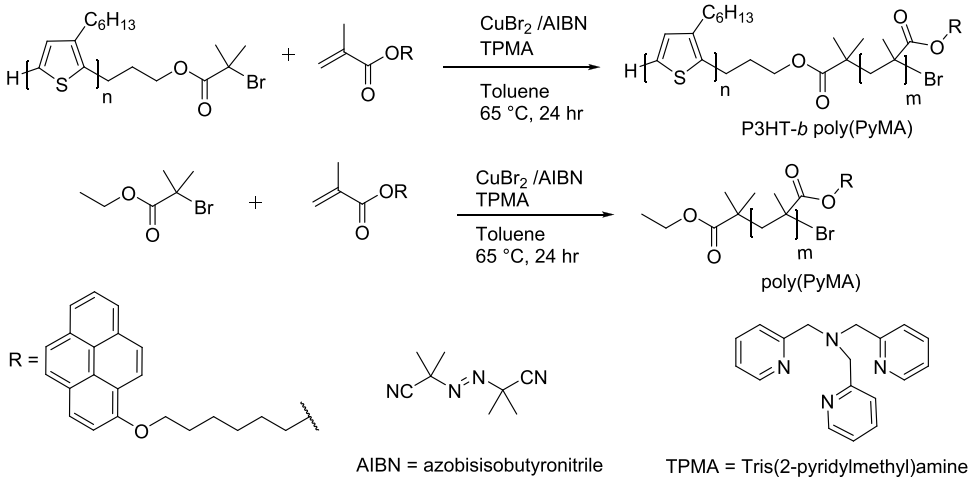

reported a series of all-conjugated triblock copolymers to comprise co-poly(3-alkylthiophene) with good electrical properties (hole mobilities > 0.1 $cm^2 V^{-1} s^{-1}$).[30]

The synthesis of poly(3-hexylthiophene)-*b*-poly(6-(pyren-1-yloxy)hexylmethacrylate) (P3HT-*b*-poly(PyMA)) reported here was accomplished by GRIM and initiators for continuous activator regeneration atom transfer radical polymerization (ICAR-ATRP).[31,32] GRIM was employed due to the ability to synthesize the P3HT block with a controlled molecular weight while maintaining the livingness of the process, high regioregularity, and low dispersity.[18,33−35] As a reversible deactivation radical polymerization (RDRP) technique, ICAR-ATRP provides the ability to tune the molar composition of the block copolymers while maintaining a narrow molecular weight distribution.[36] Thus, ICAR-ATRP was employed for the addition of the liquid crystalline block to the P3HT macroinitiator. Compared to conventional ATRP, ICAR-ATRP has the added advantage of conducting the polymerization with a lower amount of copper catalyst (<97.5%). In addition, continuous regeneration of Cu^{1+} by organic free radical generators such as azobisisobutyronitrile (AIBN) ensure continuity even in the presence of very low catalyst concentration.

Pyrene-based organic semiconducting materials have the potential to be involved in a variety of applications such as OLEDs, OFETs, and organic photovoltaics.[1−3,8,9,37] Pyrene is a chromophore with good chemical and thermal stability, high charge carrier mobility, and the capability to function as a hole injection layer, which makes it a promising material for organic electronics.[38,39] In the application of OFETs, the planar fused ring structure leads to extended conjugation and facilitates close $\pi-\pi$ stacking, resulting in high crystallinity, making pyrene an interesting material.[3,6,38,40] Thus, an array of organic semiconducting materials has been reported with the incorporation of pyrene as a substituent with the target of efficient charge transport.[3,6,38,40] The ability to undergo substitution at multiple positions and the potential of being part of large fused ring systems make pyrene a versatile building block in organic electronics that enable tuning of the structure to gain the desired properties.[8] In addition, pyrene-based blocks have been used as an effective backbone component in conjugated polymers to improve electrical properties through enhanced backbone planarity and $\pi-\pi$ stacking.[41−45]

As a thermotropic discotic liquid crystalline (LC) mesogen that can undergo columnar stacking, 6-(pyren-1-yloxy)hexyl methacrylate (PyMA) integrated into P3HT block copolymers was expected to improve ordering in the semiconducting P3HT block. In addition to providing a columnar matrix for the supramolecular self-assembly of P3HT, anisotropic charge transport of P3HT-*b*-poly(PyMA) can be further enhanced by the pyrene pendant groups due to the p-type semiconducting behavior.[4,46] The ability of PyMA to self-assemble into columnar domains during the mesophase transitions upon cooling from the isotropic state indicates the thermotropic nature of PyMA. At the same time, the flexible hexyl side chains improve solution processability into thin films and impart mechanical flexibility. The high compatibility of the two blocks with $\pi-\pi$ stacking and hole transport facilitates anisotropic long-range charge transport within the block copolymer.[3,37,46,47]

Albeit pyrene has been widely studied as a small molecule, there are not many studies related to semiconducting polymers containing pyrene as a substituent.[2,5,37,47] Among the recent works based on P3HT and pyrene, Chen et al. have reported an all-conjugated block copolymer with pyrene and P3HT, which has the potential to be used as an additive in organic photovoltaics.[48] Our group recently reported a series of side-chain thermotropic liquid-crystalline block copolymers with P3HT with calamitic mesogens.[49,50] The ability to use the well-ordered mesophases of azobenzene (nematic mesophase) and biphenyl (smectic mesophase) to enhance the self-assembly of P3HT was studied in the context of OFETs.[49,50]

In this study, we report the synthesis and characterization of the poly(3-hexylthiophene)-*b*-poly(6-(pyren-1-yloxy)hexyl methacrylate) (P3HT-*b*-poly(PyMA)) block copolymer and the homopolymer poly(PyMA). The electrical characterization of P3HT-*b*-poly(PyMA) was determined by field-effect mobility measurements (OFETs). Mesophase-driven polymer packing and the film morphology were studied and correlated with the field-effect mobility.

RESULTS AND DISCUSSION

Synthesis of Poly(3-hexylthiophene)-*b*-poly(PyMA) and Poly(PyMA). The synthesis of P3HT-*b*-poly(PyMA)

https://doi.org/10.1021/acsomega.1c04176
ACS Omega 2021, 6, 27325−27334

Table 1. Molecular Weights and Optoelectronic Properties of Polymers

polymer	M_n[a] (g mol^{-1})	PDI	λ_{max} (nm)[b]	λ_{max} (nm)[c]	optical band gap (eV)	HOMO[d] (eV)	LUMO[e] (eV)	electrochemical band gap (eV)
P3HT-Br	13,000	1.6	450	530, 604	1.90	−4.74	−2.77	1.97
P3HT-*b*-poly(PyMA)	18,000	1.7	351, 384, 450	352, 384, 525, 602	1.83	−4.83	−3.03	1.80
poly(PyMA)	3500	1.7	348, 384					

[a]Determined by SEC by calibration with polystyrene standards (THF eluent). [b]Absorption of chloroform solution. [c]Absorption of thin films annealed at 150 °C. [d]Determined from the onset of the oxidation peak of the cyclic voltammogram (CV). [e]Determined from the onset of the reduction peak of CV.

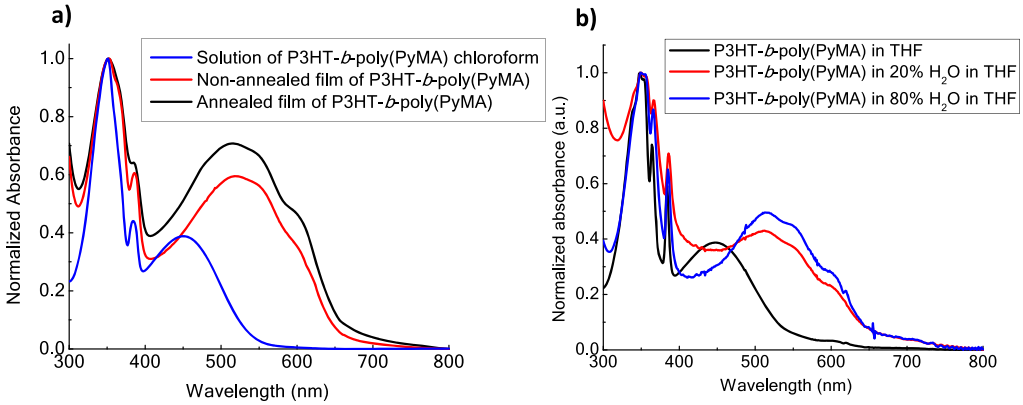

Figure 1. (a) UV−Vis absorption spectra of P3HT-*b*-poly(PyMA) and poly(PyMA) in solution and thin films (nonannealed and annealed at 150 °C for 20 min); (b) absorbance spectra for the solvatochromism study with the H_2O-THF mixture.

and poly(PyMA) was performed by ICAR-ATRP, as shown in Scheme 1. The synthesis of the P3HT macroinitiator started with the end-capping of living nickel-terminated P3HT with allyl magnesium bromide (Figure S1, Supporting Information). Allyl-terminated P3HT was subjected to hydroboration and oxidation using 9-borabicyclo[3.3.1]nonane (9-BBN) and NaOH to convert the allyl to the hydroxypropyl end group (Figure S2 and Scheme S1, Supporting Information). The reaction of hydroxypropyl-terminated P3HT with 2-bromoisobutyryl bromide in the presence of triethylamine generated the ATRP macroinitiator (P3HT-Br) (Scheme S2 and Figure S3, Supporting Information). Modification of the end groups of P3HT from allyl to hydroxypropyl to bromoester was confirmed by ^{1}H NMR analysis (Supporting Information). The vinyl protons of the allyl end group at 5.11 and 5.98 ppm disappeared with the appearance of the protons of hydroxylpropyl P3HT at 3.78 ppm. Furthermore, the appearance of a sharp singlet at 1.96 ppm (six methyl protons) indicated the formation of the bromoester ATRP macroinitiator (Supporting Information).

To synthesize P3HT-*b*-poly(PyMA) and poly(PyMA) by ICAR-ATRP, AIBN was used as the free radical generator for the activation of $CuBr_2$ by converting Cu^{2+} to Cu^{1+} in a continuous process. This method helped polymerize the methacrylate monomer with a significantly lower concentration of copper halide than our previous study.[50] With this, we overcame the need for rigorous cleaning after the conventional ATRP, which would otherwise cause residual traces of copper in the P3HT block copolymer. Furthermore, we improved the incorporation of PyMA (∼40 mol %) with a significantly lower amount of copper catalyst (97.5% less copper catalyst compared to previous studies) while maintaining a comparable PDI after the addition of the second block. This can be attributed to the reduced chain disproportionation observed in the earlier studies with conventional ATRP.[50] The content of P3HT and poly(PyMA) segments in the block copolymer was calculated from the integration of peaks of ^{1}H NMR (Supporting Information). The area under the alkoxy protons at the terminals of the hexyl side chain of PyMA units and the area under the peak for the first methylene protons attached to the thiophene ring were used to estimate the composition of each block (Figure S7, Supporting Information). The increase in the molecular weight of P3HT-*b*-poly(PyMA) as compared to the P3HT-Br macroinitiator observed in size exclusion chromatography (SEC) measurements further confirmed the incorporation of the poly(PyMA) block (Table 1 and Figure S14).

UV−Vis Analysis. The UV−Vis analysis of P3HT-Br, P3HT-*b*-poly(PyMA), and poly(PyMA) was performed both in chloroform solution and thin films (Figure 1a and Figure S9 in the Supporting Information). In the spectrum of P3HT-*b*-poly(PyMA) in chloroform, the peak at 450 nm corresponds to the P3HT block, while the peaks at 351 and 384 nm are attributed to the absorption by pyrene. The well-defined peak at 351 nm is due to $S_0 \rightarrow S_2$ transition of the methacrylate-bound pyrene units, and the less intense peak at 384 nm corresponds to the weaker transition from $S_0 \rightarrow S_1$. The absorption peaks of pyrene red-shifted for the films of P3HT-*b*-poly(PyMA) under both annealed and nonannealed conditions, indicating closer π stacking of pyrene units upon crystallization. In addition, the peak at 525 nm in the nonannealed thin-film spectrum of P3HT-*b*-poly(PyMA) corresponds to $\pi-\pi^*$ transition in the P3HT block, which shows a clear redshift of ∼75 nm (Figure 1 a) when moving from solution to a thin film. Compared to the solution, this is due to the enhanced ordering in the P3HT block copolymer films. The vibronic structure of the absorption band of the solid film becomes more distinct with the appearance of the

https://doi.org/10.1021/acsomega.1c04176
ACS Omega 2021, 6, 27325−27334

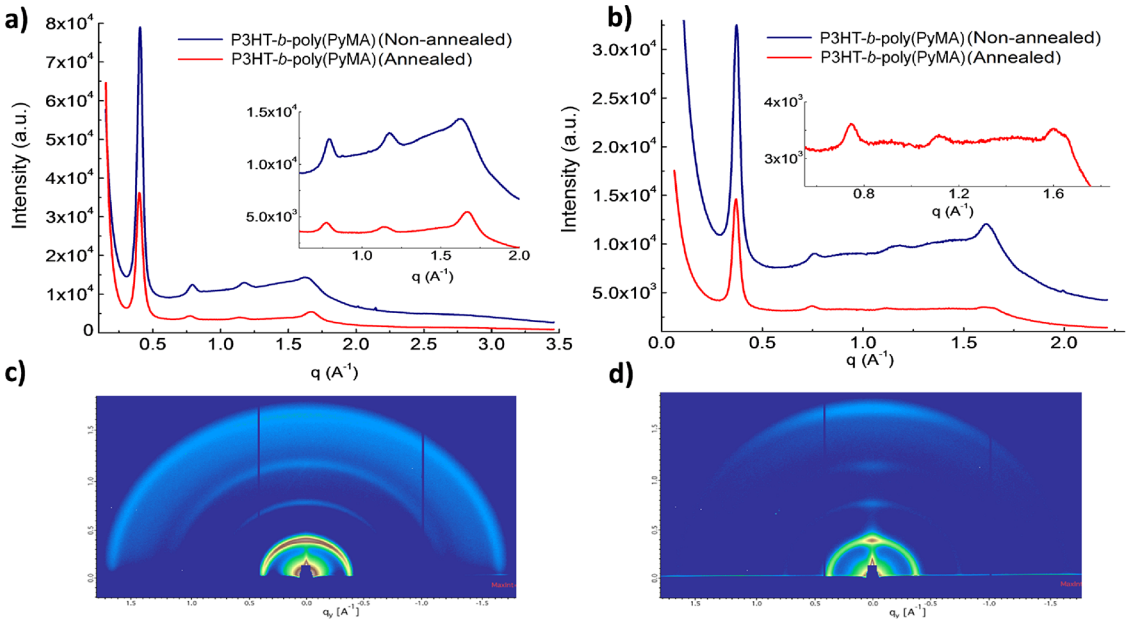

Figure 2. 2D GIWAXS data of P3HT-*b*-poly(PyMA) deposited from chlorobenzene on SiO_2 substrates: (a) out-of-plane and (b) in-plane sector cuts. 2D GIWAXS patterns of P3HT-*b*-poly(PyMA) (c) before annealing and (d) after annealing at 150 °C for 20 min.

peak at 602 nm upon annealing films of P3HT-*b*-poly(PyMA) (Figure 1a). Annealing of this crystalline block copolymer has created an improved ordering in thin films, leading to improved interchain $\pi-\pi$ stacking interactions.

Solvatochromism of the P3HT-*b*-poly(PyMA) diblock copolymer was studied with a series of solution mixtures of THF and H_2O (Figure 1b, Figure S11, and Table S1 in the Supporting Information) in which P3HT-*b*-poly(PyMA) is fully soluble in THF and insoluble in H_2O. The concentration of P3HT was kept constant throughout the solution series with the incremental addition of water to the solvent mixture. It was observed that the absorbance spectra were red-shifted, indicating the solvent-induced aggregation of polymer chains, resulting in positive solvatochromism (Figure S11, Supporting Information). At the THF:H_2O volume ratio of 10:90, P3HT-*b*-poly(PyMA) became utterly insoluble in the solvent mixture. According to our previous study, the solubility of P3HT-*b*-poly(PyMA) is higher than that of the precursor P3HT (P3HT-Br).[28] This can be attributed to the favorable interactions of water with multiple ester linkages of methacrylate units in the second block. The hydrophobic P3HT segment can get shielded with the LC block. Close stacking of P3HT chains within the aggregates could have resulted in the fine vibronic structure of the absorption spectra, independent of the concentration. The water content λ_{max} increment corresponding to the P3HT block has red-shifted by ~68 nm. Furthermore, the absorbance peak for pyrene developed into the fine vibronic structure, indicating $\pi-\pi$ stacking in both blocks within the potential aggregate formation.[28] Cyclic voltammetry was used to estimate the HOMO and LUMO energy levels of P3HT-*b*-poly(PyMA) from the potential onset values of oxidation and reduction curves, respectively (Table 1). For P3HT-*b*-poly(PyMA), the stabilization of the LUMO level in the block copolymer has accounted for a decline in the band gap after adding the LC block. Both P3HT-*b*-poly(PyMA) and P3HT-Br have comparable electrochemical band gaps where the insulating liquid crystalline block did not significantly diminish the charge transport properties (Figure S10, Supporting Information).

X-ray Diffraction Studies. The crystallinity of P3HT-*b*-poly(PyMA) concerning lamellae packing and $\pi-\pi$ stacking was studied both under annealed and nonannealed conditions using 2D grazing-incidence wide-angle X-ray scattering (GIWAXS) (Figure 2) and grazing-incidence small-angle X-ray scattering (GISAXS) (Figure S12, Supporting Information) data. The GIWAXS data show long-range order and $\pi-\pi$ stacking corresponding to P3HT crystals for annealed and nonannealed films. Before annealing, crystallites are mostly nontextured such that crystals are isotropically oriented. After annealing, the (100) intensity appears to be more localized to the out-of-plane direction, although a significant amount of $\pi-\pi$ stacking is also apparent.

Both out-of-plane and in-plane sector cuts showed a decrease in the (100) peak with annealing. Because GIWAXS data cannot capture crystals strongly textured in the out-of-plane direction (within a few degrees), we attributed the apparent loss in GIWAXS intensity for the (100) peak to the formation of crystals with lamellar stacking that is highly oriented in the out-of-plane direction. With annealing, sector cuts in Figure 2 also showed an increase in the $\pi-\pi$ stacking peak in the out-of-plane direction and decreased in-plane peak intensity. This suggests that annealing leads to stronger "face-on" stacking. Furthermore, the d-spacing between the polymers decreased from 3.90 Å to 3.75 Å, indicating dense packing of polymer chains that could facilitate charge hopping within the semiconducting P3HT block. Close lamellae stacking of polymer chains of P3HT-*b*-poly(PyMA) was observed in thin-film XRD analysis performed on films of P3HT-*b*-poly(PyMA) and P3HT-Br on silicon substrates to explore the packing arrangements and crystallinity (Figure S13 and Table S2, Supporting Information). Closely resembling XRD spectra of P3HT-*b*-poly(PyMA) and P3HT-Br indicated unaltered π stacking and lamellar stacking of the P3HT segment in P3HT-*b*-poly(PyMA) even after the addition of the LC segment. Furthermore, the lamellae packing distance in

https://doi.org/10.1021/acsomega.1c04176
ACS Omega 2021, 6, 27325−27334

P3HT-*b*-poly(PyMA) was reduced by 3.22 Å compared to P3HT-Br (Figure S13 and Table S2, Supporting Information). This increased close assembly of P3HT-*b*-poly(PyMA) explains the comparable hole mobility in OFETs for P3HT-*b*-poly(PyMA) with its macroinitiator (P3HT-Br) even in the presence of an insulating methacrylate block.

GISAXS data (Figure S12, Supporting Information) of P3HT-*b*-poly(PyMA) did not show any peaks that can be attributed to microphase-separated domains, suggesting that the two blocks are uniformly dispersed within the films even upon annealing.

Field-Effect Mobility. Field-effect mobilities (μ) of P3HT-*b*-poly(PyMA) were measured in a bottom-gate, top-contact field-effect transistor (OFET) using the equation:

$$\mu = \frac{2L}{WC_i}\left[\frac{I_{DS}}{(V_{GS} - V_T)^2}\right]$$

where I_{DS} is the source−drain current, V_{GS} is the gate voltage, V_T is the threshold voltage, C_i is the capacitance of the dielectric, W is the channel width, and L is the channel length. OFET measurements were performed under both nontreated and (heptadecafluoro-1,1,2,2-tetrahydrodecyl)trimethoxysilane (FTS)-treated SiO_2 dielectric conditions for both the P3HT macroinitiator and P3HT-*b*-poly(PyMA) diblock copolymer. The average field-effect mobilities obtained for both polymers are listed in Table 2 (see Figure 3 and Figure S15 in the Supporting Information).

Table 2. Field-Effect Mobilities Were Obtained for P3HT-*b*-poly(PyMA) and P3HT-Br for FTS-Treated and Nontreated OFET Devices

polymer	device	average V_T (V)	I_{on}/I_{off}	average mobility ($cm^2 V^{-1} s^{-1}$)[a]
P3HT-Br	nontreated	15.5 ± 0.8	10^3	1.00×10^{-2} (1.11×10^{-2})
	FTS-treated	5.2 ± 1.3	10^3	1.21×10^{-2} (1.34×10^{-2})
P3HT-*b*-poly(PyMA)	nontreated	11.2 ± 2.1	10^3	8.54×10^{-3} (8.76×10^{-3})
	FTS-treated	12.5 ± 1.2	10^3	1.53×10^{-2} (2.16×10^{-2})

[a]Measured for 15 devices annealed at 150 °C for 20 min; maximum field-effect mobilities measured are given in brackets.

The highest hole mobilities measured for P3HT-*b*-poly(PyMA) were 8.76×10^{-3} cm^2 V^{-1} s^{-1} for nontreated devices and 2.16×10^{-2} cm^2 V^{-1} s^{-1} for FTS-treated devices. According to the UV−Vis and XRD studies, both treated and nontreated devices were annealed at 150 °C for 20 min before measurements for better packing of the block copolymer. The average field-effect mobility of P3HT-*b*-poly(PyMA) was comparable with that of the P3HT macroinitiator after the surface treatment with FTS. The increased hydrophobicity of the SiO_2 surface with FTS treatment helped form favorable hydrophobic surface interactions with P3HT and pyrene units. This facilitated the increase in the mobility of P3HT-*b*-poly(PyMA) compared to the nontreated devices. Favorable surface interactions and annealing above the mesophase transition help the pyrene units in the methacrylate block undergo columnar stacking and contribute to the charge transport.[47] There are no indication of nanofibril formation in P3HT-*b*-poly(PyMA) films (as in pristine P3HT) observed in tapping mode atomic force microscopy (TMAFM) (Figure 4 and Figure S16). Yet, the contribution from pyrene in charge transport could have contributed to the comparable OFET results of P3HT-*b*-poly(PyMA) and pristine P3HT.[51] The threshold voltages to turn on devices are somewhat higher, although this could be due to the oxidation of the polymers since the measurements were performed under ambient conditions.

Surface Morphology. TMAFM analysis was performed on the thin films of P3HT-*b*-poly(PyMA) and the macroinitiator (P3HT-Br) both on mica and in the OFET channel region. Sample preparation on mica was performed by drop-casting solutions of P3HT-*b*-poly(PyMA) in chlorobenzene (0.3 mg mL^{-1}). Slow evaporation of the solvent is expected to provide sufficient time for the polymer chains to undergo adequate packing followed by annealing at 150 °C for 20 min. The unique morphology of P3HT-*b*-poly(PyMA) was observed on mica for both annealed and nonannealed conditions (Figure 4). The characteristic nanofibrillar morphology of P3HT was only observed in the macroinitiator films on mica (Figure 4 and Figure S16). Yet, the unique morphology observed for P3HT-*b*-poly(PyMA) appeared to be consistent for a long range (~20 μm) both on mica and silicon wafers (Figure 4).

The correlation between the appearance of the microstructure and higher values for the field-effect mobility suggests that the morphological features positively contribute to long-range ordering. It is plausible that the organization of the pyrene pendant groups into columnar assemblies after annealing creates a matrix in which the rigid polythiophene chains can organize.[52−54] In addition, the FTS-treated OFET surface had more uniformity and smoother morphology as compared to the nontreated device surface, indicating better surface interactions of P3HT-*b*-poly(PyMA) with the FTS-modified SiO_2 dielectric surface, leading to more even and ordered distribution of the polymer within the channel region of the OFETs (see Figure S16 in the Supporting Information).

Thermotropic Phase Behavior and Liquid Crystallinity. The thermal transitions of P3HT-*b*-poly(PyMA), including the glass transition, melting point, crystallization, and mesophase transitions, were studied with DSC. The data were collected from the first cooling and second heating curves. Prominent first-order transitions were observed for melting (198 °C) (Figure S17) and crystallization (166 °C) (Figure S18) of P3HT-*b*-poly(PyMA), respectively, in the heating and cooling curves. The second-order transition at 77 °C is the glass transition of the methacrylate block. The weak endothermic transition at ~125 °C in the cooling curve is due to the LC mesophase transition of pyrene (Figure S18). The presence of the mesophase transition of pyrene after the glass transitions of the methacrylate block provides more flexibility for the mesogens to undergo rearrangements using heat as a trigger. After passing the glass transition, the polymer behaves like a more rubbery and flexible medium. This helps the alignment of the mesogenic groups at the mesophase transition, which is due to the increased mobility within the medium. As a result, upon cooling from the mesophase transition temperature, pyrene can undergo long-range $\pi-\pi$ stacking. After cooling below the crystallization temperature, the block copolymer becomes more rigid and crystalline, and the long-range assembly will remain intact, enhancing the OFET performance of P3HT-*b*-poly(PyMA).

Thin films for the polarized optical microscopy of P3HT-*b*-poly(PyMA) and poly(PyMA) were spin-coated on clean glass

https://doi.org/10.1021/acsomega.1c04176
ACS Omega 2021, 6, 27325−27334

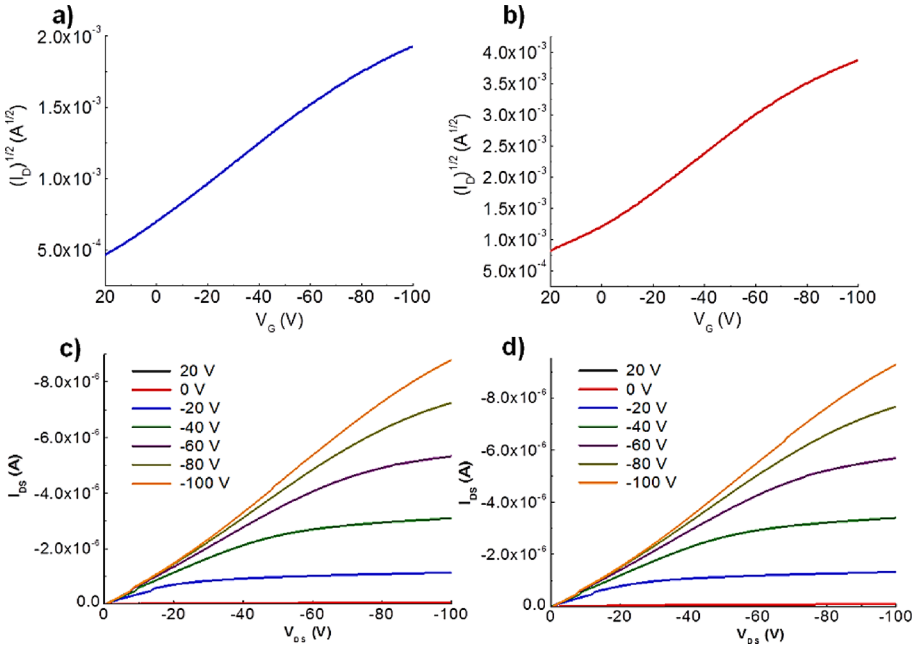

Figure 3. Transfer curves of (a) P3HT-*b*-poly(PyMA) nontreated OFETs and (b) P3HT-*b*-poly(PyMA) FTS-treated OFETs; output curves of (c) P3HT-*b*-poly(PyMA) nontreated OFETs and (d) P3HT-*b*-poly(PyMA) FTS-treated OFETs at V_{DS} = −100 V (W = 530 μm, L = 50 μm).

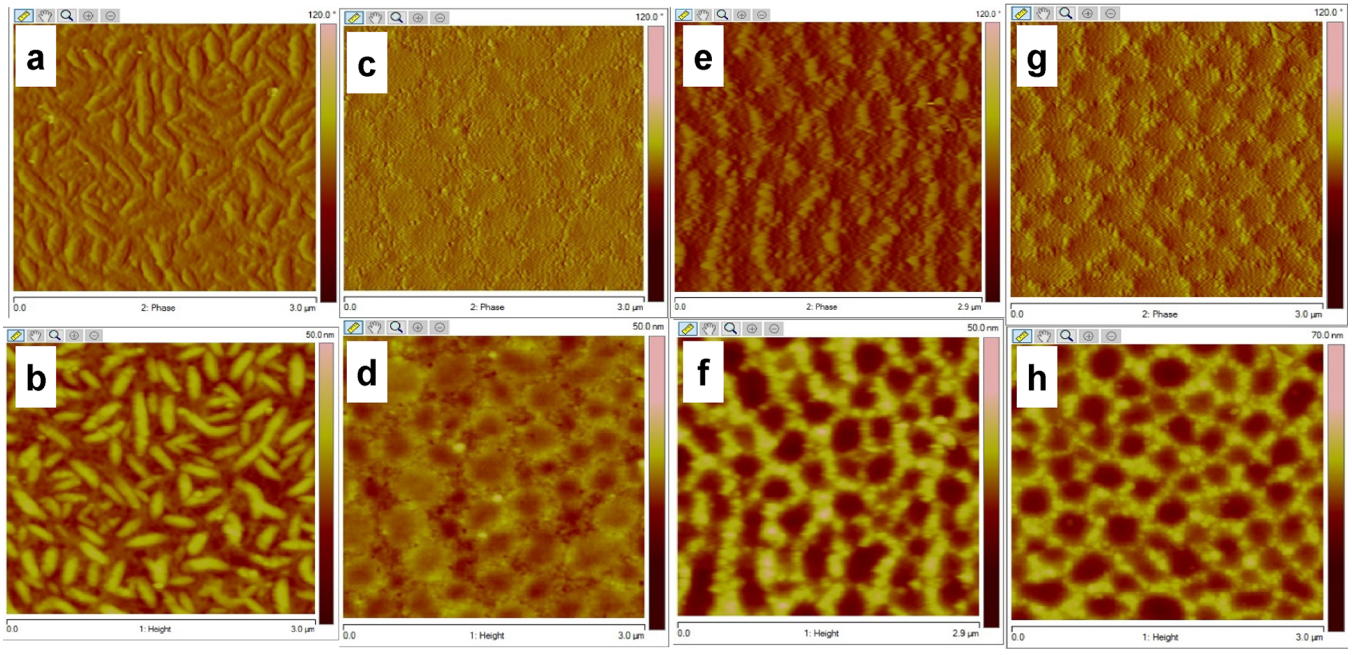

Figure 4. TMAFM (3 μm × 3 μm) (a) phase and (b) height images of P3HT-Br (R_q = 0.8); (c) phase and (d) height images of P3HT-*b*-poly(PyMA) on mica (R_q = 1.1); (e) phase and (f) height images of P3HT-*b*-poly(PyMA) on nontreated OFET devices (R_q = 1.7); (g) phase and (h) height images of P3HT-*b*-poly(PyMA) on FTS-treated OFET devices (R_q = 1.5).

surfaces from solutions in chlorobenzene. The films were heated up to the isotropic state (150 °C) using the heating stage. Afterward, samples were allowed to cool slowly up to the mesophase transition temperature range that was obtained from the DSC analysis. The micrographs were collected under the cross-polarizer under high power (400× magnification) (Figure 5).

PyMA is a discotic LC mesogen with a rigid core of pyrene ring connected to methacrylate via a six-carbon flexible side chain. Due to the conjugated planar core of pyrene that can undergo $\pi-\pi$ stacking, it can facilitate charge transport by hopping between the adjacent units.[46] Thus, pyrene is an interesting mesogen for organic electronic applications as compared to the calamitic mesogens used in our previous studies, which are not capable of charge transport.[28,49,50,55] Also, this can be correlated with the comparable hole mobility of P3HT-*b*-poly(PyMA) with the macroinitiator, which was not observed with the calamitic mesogens in our previous studies.[49,50] By comparing the POM images before and after the mesophase transition, it can be observed that the polymer films gained an extended uniform pattern after heating and crystallization (Figure 5). The less defined and randomly

https://doi.org/10.1021/acsomega.1c04176
ACS Omega 2021, 6, 27325−27334

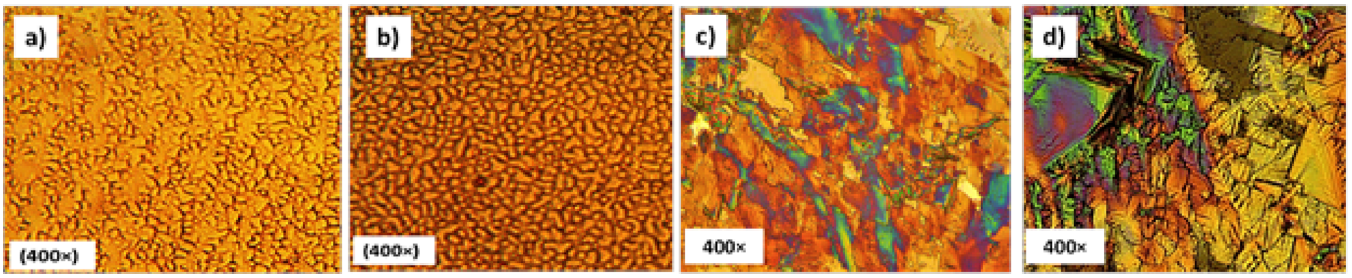

Figure 5. Polarized optical micrographs of P3HT-*b*-poly(PyMA) (a) before heating (b) during mesophase transition (~130 °C) after cooling from the isotropic state and polarized optical micrographs of poly(PyMA) (c) before heating (d) during mesophase transition (~130 °C) after cooling from the isotropic state.

distributed domains become more defined after cooling below the mesophase transition (Figure 5). The characteristic discotic mesophase features observed in the poly(PyMA) homopolymer is less prominent in P3HT-*b*-poly(PyMA) due to the high content of P3HT (60 mol %). Yet, the POM images demonstrated good consistency with the TMAFM images of P3HT-*b*-poly(PyMA) after annealing, which indicated long-range ordering in P3HT-*b*-poly(PyMA).

METHODS

Materials. All commercially available chemicals were obtained from Aldrich Chemical Co. Inc. No further purifications were done unless noted otherwise. All the glassware was oven-dried before the experiments, and reactions were performed under an inert nitrogen environment. The glassware used for the polymerization was oven-dried at 120 °C and cooled under nitrogen before the experiment. Freshly distilled tetrahydrofuran (THF) obtained after drying over sodium benzophenone ketyl was used in reactions.

General Characterization Methods. A detailed description of all the general characterization methods is provided in the Supporting Information. Briefly, monomer and polymer structures were characterized using nuclear magnetic resonance (NMR) spectroscopy, gas chromatography−mass spectrometry (GC−MS) (for monomers), and size exclusion chromatography (SEC) (for polymers). The thermal properties of the materials were analyzed by DSC. Furthermore, cyclic voltammetry and UV−Vis spectroscopy were employed in determining optoelectronic properties. OFET properties were analyzed by preparing thin-film transistors with the bottom-gate, top-contact configuration at different annealing temperatures, and transfer and output characteristics were determined. Thin-film properties were further investigated by TMAFM, POM, GIWAXS, and thin-film XRD.

Synthesis of the Liquid Crystalline Monomer (PyMA). The discotic mesogen 6-(pyren-1-yloxy)hexyl methacrylate (PyMA) was synthesized using pyrene-1-carbaldehyde (10.00 g, 0.044 mol) as the starting material. The conversion of pyrene-1-carbaldehyde to pyren-1-ol (Figure S4) was done according to the procedure reported by Chen and co-workers (6.72 g; yield, 70%).[48] ^{1}H NMR ($CDCl_3$, 500 MHz): δ 7.34−8.61 (m, 9H), 5.60 (broad s, 1H).

Synthesis of 1-((6-Bromohexyl)oxy)pyrene. Pure pyren-1-ol (6.72 g, 0.031 mol) was subjected to Williamson ether synthesis in the presence of 1,6-dibromohexane (9.54 mL, 0.062 mol) and K_2CO_3 (5.53 g, 0.04 mol) using acetone (250 mL) as the solvent. The reaction mixture was refluxed for 24 h at 65 °C. The resulting solution was filtered hot using vacuum filtration to remove K_2CO_3 and was concentrated under reduced pressure. Petroleum ether was added to the resulting concentrated solution to separate the product 1-((6-bromohexyl)oxy)pyrene (Figure S5). The solid product was isolated by gravity filtration and further purified by recrystallization from methanol (8.72 g; yield, 74%). ^{1}H NMR ($CDCl_3$, 500 MHz): δ 7.48−8.53 (m, 9H), 4.33 (t, 2H), 2.15 (t, 2H), 2.03 (m, 2H), 1.96 (m, 2H), 1.69 (m, 2H), 1.61 (m, 2H).

Synthesis of 6-(Pyren-1-yloxy)hexyl Methacrylate. Potassium methacrylate was prepared by adding methacrylic acid (2.58 g, 0.030 mol) dropwise into $KHCO_3$ (3.00 g, 0.030 mol, 100 mL) aqueous solution. Pure 1-((6-bromohexyl)oxy)-pyrene (8.72 g, 0.023 mol) was reacted with excess potassium methacrylate in the presence of hydroquinone (0.25 mg g, 0.0023 mol). *N*,*N*′-Dimethylformamide (DMF) (300 mL) was used as the solvent, and the reaction mixture was refluxed at 100 °C for 24 h. Excess distilled water was added to the resulting reaction mixture after cooling to precipitate 6-(pyren-1-yloxy)hexyl methacrylate (PyMA) (Figure S6). The product was isolated from gravity filtration, dissolved in $CHCl_3$, and washed further with 5% NaOH aqueous solution and distilled water to remove the remaining residual methacrylic acid and salts in PyMA. Then, the organic layer was dried over anhydrous $MgSO_4$ and was concentrated under reduced pressure. The solid PyMA obtained was further purified by recrystallization from ethanol (7.46 g, yield 84%). ^{1}H NMR ($CDCl_3$, 500 MHz): δ 7.48−8.53 (m, 9H), 5.98 (s, 1H), 5.51 (s, 1H), 4.35 (t, 2H), 4.20 (t, 2H), 4.36 (t, 2H), 4.23 (t, 2H), 2.00 (m, 2H), 1.95 (m, 3H), 1.75 (m, 2H), 1.72 (m, 2H), 1.56 (m, 2H).

Synthesis of the P3HT Macroinitiator (P3HT-Br). The synthesis of allyl end-capped P3HT, hydroxypropyl end-capped P3HT precursors (Scheme S1), and P3HT-Br is given in the Supporting Information.

Synthesis of Poly(3-hexylthiophene)-*b*-poly(PyMA). P3HT-Br was subjected to ICAR-ATRP with the LC monomer (PyMA), Cu catalyst ($CuBr_2$), chelating ligand tris[(2-pyridyl)methyl]amine (TPMA), and the radical initiator (AIBN). A clean dry Schlenk flask was charged with P3HT-Br (0.5 g, 0.0385 mmol), PyMA (2.97 g, 7.7 mmol), $CuBr_2$ (0.430 mg, 0.0019 mmol), TPMA (2.236 mg, 0.0077 mmol), and AIBN (1.264 mg, 0.0077 mmol). Therefore, the molar ratio of the reactants is PYMA:P3HT:$CuBr_2$:TPMA:AIBN = 200:1:0.05:0.2:0.2. After subjecting the reaction mixture to three freeze−pump−thaw cycles, the Schlenk flask was immersed in a thermostat oil bath at 65 °C. A minimum amount of toluene (~4 mL) was used as the solvent. The reaction mixture was stirred under nitrogen for 24 h at 65 °C. The formation of the second block was confirmed by

https://doi.org/10.1021/acsomega.1c04176
ACS Omega 2021, 6, 27325−27334

withdrawing samples from the reaction mixture using deoxygenated syringes and isolating the polymer by precipitating in methanol. After 24 h, the reaction mixture was precipitated in cold methanol to isolate P3HT-*b*-poly(PyMA). Further purification was done by reprecipitation of P3HT-*b*-poly(PyMA) in excess methanol after dissolving in THF, followed by drying under vacuum until the complete removal of solvent residues. Polymer characterization was done by SEC (M_n = 18,000 g mol^{-1}, PDI = 1.7) and ^{1}H NMR (Figure S7 in the Supporting Information). Percent yield = 53%. ^{1}H NMR (500 MHz, $CDCl_3$): δ H 0.92 (s, 3H), 1.12−1.63 (m, 6H), 1.69 (t, 2H), 2.80 (t, 2H), 3.68 (s, 3H), 3.86 (s, 4H), 6.96 (s, 1H), 6.75−8.45 (broad peaks for pyrene protons, 9H). SEC: M_n = 18,000 g mol^{-1}; PDI = 1.7.

Synthesis of Poly(PyMA). PyMA was polymerized by ICAR-ATRP following the same experimental procedure as in P3HT-*b*-poly(PyMA). Poly(PyMA) was synthesized using the LC monomer PyMA (2.97 g, 7.7 mmol), ethyl 2-bromoisobuterate (EBiB) (7.5 mg, 0.0385 mmol), $CuBr_2$ (0.086 mg, 0.385 μmol), TPMA (0.447 mg, 1.54 μmol), and the radical initiator AIBN (0.253 mg, 1.54 μmol). A clean, dry Schlenk flask was charged with all the reactants with 4 mL of toluene in the molar ratio of PYMA:EBiB:$CuBr_2$:TPMA:AIBN = 200:1:0.01:0.04:0.04. After three freeze−pump−thaw cycles, the Schlenk flask was immersed in a thermostat oil bath at 65 °C for 24 h under nitrogen with stirring. The resulting polymer was further purified by reprecipitation in cold methanol from a solution of poly(PyMA) in THF before characterization by SEC and ^{1}H NMR (Figure S8 in the Supporting Information). Percent yield = 63%. ^{1}H NMR ($CDCl_3$, 500 MHz): δ 6.8−8.5 (m, 9H), 3.8 (broad s, 4H), 0.7−2.3 (m, 10H), 0.95 (s, 3H). SEC: M_n = 3500 g mol^{-1}, PDI = 1.7.

CONCLUSIONS

A poly(3-hexylthiophene)-*b*-poly(PyMA) diblock copolymer and poly(PyMA) homopolymer carrying pendant pyrene units as thermotropic discotic LC mesogens were synthesized and characterized. In comparison with previous studies, employing ICAR-ATRP contributed to the significant reduction of the amount of copper catalyst (<97.5%) required for the addition of the second block while maintaining comparatively low PDI. Well-ordered packing of the polymer was confirmed by UV−Vis analysis, XRD data, and TMAFM studies. The thermotropic liquid crystallinity of poly(3-hexylthiophene)-*b*-poly(PyMA) with the formation of the discotic mesophase was investigated and confirmed with DSC and POM. Annealing above the mesophase transition led to a long-range order in poly(3-hexylthiophene)-*b*-poly(PyMA) in the active layer of OFETs, improving self-assembly, resulting in comparable field-effect mobilities with the P3HT macroinitiator (in the order of 10^{-2} cm^2 V^{-1} s^{-1}), even in the presence of the insulating LC block. Our results demonstrate a path to control block copolymer morphologies with potential applications in displays, sensors, and memory devices.

ASSOCIATED CONTENT

Supporting Information

The Supporting Information is available free of charge at https://pubs.acs.org/doi/10.1021/acsomega.1c04176.

General characterization methods; synthesis procedures (allyl-terminated P3HT, hydroxypropyl-terminated P3HT, and P3HT macroinitiator); ^{1}H NMR spectra (allyl-terminated P3HT, hydroxypropyl-terminated P3HT, monobromoester-terminated P3HT, P3HT macroinitiator, pyren-1-ol, 1-((6-bromohexyl)oxy)-pyrene, 6-(pyren-1-yloxy)hexyl methacrylate (PyMA), P3HT-*b*-poly(PyMA), and poly(PyMA)); UV−Vis absorption spectra of P3HT-Br; CVs of P3HT-Br and P3HT-*b*-PyMA; solvatochromism study; GISAXS data of P3HT-*b*-poly(PyMA); thin-film XRD spectra of P3HT-*b*-poly(PyMA); GPS traces of polymers P3HT-Br and P3HT-*b*-poly(PyMA); transfer and output curves of P3HT-Br nontreated and P3HT-Br FTS-treated devices; 3D TMAFM images of polymer thin films; DSC thermograms of polymers (PDF)

AUTHOR INFORMATION

Corresponding Author

Mihaela C. Stefan − *Department of Chemistry and Biochemistry, University of Texas at Dallas, Richardson, Texas 75080, United States;* orcid.org/0000-0003-2475-4635; Email: mihaela@utdallas.edu

Authors

Taniya M. S. K. Pathiranage − *Department of Chemistry and Biochemistry, University of Texas at Dallas, Richardson, Texas 75080, United States*

Ziyuan Ma − *Department of Chemistry and Biochemistry, University of Texas at Dallas, Richardson, Texas 75080, United States*

Chinthaka M. Udamulle Gedara − *Department of Chemistry and Biochemistry, University of Texas at Dallas, Richardson, Texas 75080, United States*

Xiangcheng Pan − *Center for Macromolecular Engineering, Department of Chemistry, Carnegie Mellon University, Pittsburgh, Pennsylvania 15213, United States;* orcid.org/0000-0003-3344-4639

Youngmin Lee − *Department of Chemical Engineering, The New Mexico Institute of Mining and Technology, Socorro, New Mexico 87801, United States;* orcid.org/0000-0002-7402-8829

Enrique D. Gomez − *Department of Chemical Engineering, The New Mexico Institute of Mining and Technology, Socorro, New Mexico 87801, United States; Department of Chemical Engineering, Department of Materials Science and Engineering, and Materials Research Institute, The Pennsylvania State University, University Park, Pennsylvania 16802, United States;* orcid.org/0000-0001-8942-4480

Michael C. Biewer − *Department of Chemistry and Biochemistry, University of Texas at Dallas, Richardson, Texas 75080, United States*

Krzysztof Matyjaszewski − *Center for Macromolecular Engineering, Department of Chemistry, Carnegie Mellon University, Pittsburgh, Pennsylvania 15213, United States;* orcid.org/0000-0003-1960-3402

Complete contact information is available at: https://pubs.acs.org/10.1021/acsomega.1c04176

Author Contributions

The manuscript was written through the contributions of all authors. All authors have approved the final version of the manuscript.

Notes

The authors declare no competing financial interest.

https://doi.org/10.1021/acsomega.1c04176
ACS Omega 2021, 6, 27325−27334

■ ACKNOWLEDGMENTS

Funding from Welch Foundation (AT-1740) and National Science Foundation (CHE-1566059 and CHE-1609880) is gratefully acknowledged (M.C.S.). M.C.S. thanks the generous endowed chair support from the Eugene McDermott Foundation. Y.L. and E.D.G. acknowledge the Office of Naval Research for financial support under grant no. N00014-17-1-2214. The Advanced Light Source is an Office of Science User Facility operated for the U.S. Department of Energy Office of Science by Lawrence Berkeley National Laboratory and is supported by the U.S. Department of Energy under contract no. DE-AC02-05CH11231.

■ REFERENCES

(1) Cominetti, A.; Pellegrino, A.; Longo, L.; Po, R.; Tacca, A.; Carbonera, C.; Salvalaggio, M.; Baldrighi, M.; Meille, S. V. Polymer solar cells based on poly(3-hexylthiophene) and fullerene: Pyrene acceptor systems. *Mater. Chem. Phys.* **2015**, *159*, 46−55.

(2) Kwon, J.; Hong, J.-P.; Noh, S.; Kim, T.-M.; Kim, J.-J.; Lee, C.; Lee, S.; Hong, J.-I. Pyrene end-capped oligothiophene derivatives for organic thin-film transistors and organic solar cells. *New J. Chem.* **2012**, *36*, 1813−1818.

(3) Figueira-Duarte, T. M.; Müllen, K. Pyrene-Based Materials for Organic Electronics. *Chem. Rev.* **2011**, *111*, 7260−7314.

(4) Zhang, H.; Wang, Y.; Shao, K.; Liu, Y.; Chen, S.; Qiu, W.; Sun, X.; Qi, T.; Ma, Y.; Yu, G.; Su, Z.; Zhu, D. Novel butterfly pyrene-based organic semiconductors for field effect transistors. *Chem. Commun.* **2006**, 755−757.

(5) Constantinescu, C.; Diallo, A. K.; D'Aleo, A.; Fages, F.; Rotaru, P.; Videlot-Ackermann, C.; Delaporte, P.; Alloncle, A.-P. Thermal behaviour and thin film properties of a bis-pyrene compound for organic thin film transistor applications. *Synth. Met.* **2015**, *209*, 29−33.

(6) Cho, H.; Lee, S.; Cho, N. S.; Jabbour, G. E.; Kwak, J.; Hwang, D.-H.; Lee, C. High-Mobility Pyrene-Based Semiconductor for Organic Thin-Film Transistors. *ACS Appl. Mater. Interfaces* **2013**, *5*, 3855−3860.

(7) Kwon, J.; Hong, J.-P.; Lee, W.; Noh, S.; Lee, C.; Lee, S.; Hong, J.-I. Naphtho[2,3,a]pyrene as an efficient multifunctional organic semiconductor for organic solar cells, organic light-emitting diodes, and organic thin-film transistors. *Org. Electron.* **2010**, *11*, 1103−1110.

(8) Sonar, P.; Soh, M. S.; Cheng, Y. H.; Henssler, J. T.; Sellinger, A. 1,3,6,8-Tetrasubstituted Pyrenes: Solution-Processable Materials for Application in Organic Electronics. *Org. Lett.* **2010**, *12*, 3292−3295.

(9) Lai, S. L.; Tong, Q. X.; Chan, M. Y.; Ng, T. W.; Lo, M. F.; Ko, C. C.; Lee, S. T.; Lee, C. S. Carbazole−pyrene derivatives for undoped organic light-emitting devices. *Org. Electron.* **2011**, *12*, 541−546.

(10) Yi, J.-P.; Zhao, L.; Xu, W.; Liu, C.-F.; Lai, W.-Y.; Huang, W. Pyrene-capped starburst emitters as gain media for organic lasers: design, synthesis, and stabilized lasing properties. *J. Mater. Chem. C* **2016**, *4*, 7546−7553.

(11) Sang, M.; Cao, S.; Yi, J.; Huang, J.; Lai, W.-Y.; Huang, W. Multi-substituted triazatruxene-functionalized pyrene derivatives as efficient organic laser gain media. *RSC Adv.* **2016**, *6*, 6266−6275.

(12) Liang, J.; Su, Y.; Lin, Q.; Zhou, H.; Zhang, S.; Pei, Y.; Hu, R. Forming-free resistive switching memory based on LiFePO 4 nanoparticle embedded in conjugated polymer. *Semicond. Sci. Technol.* **2014**, *29*, 115029.

(13) Liu, J.; Yin, Z.; Cao, X.; Zhao, F.; Lin, A.; Xie, L.; Fan, Q.; Boey, F.; Zhang, H.; Huang, W. Bulk Heterojunction Polymer Memory Devices with Reduced Graphene Oxide as Electrodes. *ACS Nano* **2010**, *4*, 3987−3992.

(14) McCullough, R. D. The Chemistry of Conducting Polythiophenes. *Adv. Mater.* **1998**, *10*, 93−116.

(15) Pathiranage, T. M. S. K.; Magurudeniya, H. D.; Biewer, M. C.; Stefan, M. C. Effect of thiophene spacers in benzodithiophene-based polymers for organic electronics. *J. Polym. Sci., Part A: Polym. Chem.* **2017**, *55*, 3942−3948.

(16) Zhang, R.; Li, B.; Iovu, M. C.; Jeffries-El, M.; Sauvé, G.; Cooper, J.; Jia, S.; Tristram-Nagle, S.; Smilgies, D. M.; Lambeth, D. N.; McCullough, R. D.; Kowalewski, T. Nanostructure Dependence of Field-Effect Mobility in Regioregular Poly(3-hexylthiophene) Thin Film Field Effect Transistors. *J. Am. Chem. Soc.* **2006**, *128*, 3480−3481.

(17) Pathiranage, T. M. S. K.; Dissanayake, D. S.; Niermann, C. N.; Ren, Y.; Biewer, M. C.; Stefan, M. C. Role of polythiophenes as electroactive materials. *J. Polym. Sci., Part A: Polym. Chem.* **2017**, *55*, 3327−3346.

(18) Stefan, M. C.; Bhatt, M. P.; Sista, P.; Magurudeniya, H. D. Grignard metathesis (GRIM) polymerization for the synthesis of conjugated block copolymers containing regioregular poly(3-hexylthiophene). *Polym. Chem.* **2012**, *3*, 1693−1701.

(19) Bhatt, M. P.; Magurudeniya, H. D.; Rainbolt, E. A.; Huang, P.; Dissanayake, D. S.; Biewer, M. C.; Stefan, M. C. Poly(3-Hexylthiophene) Nanostructured Materials for Organic Electronics Applications. *J. Nanosci. Nanotechnol.* **2014**, *14*, 1033−1050.

(20) Alemseghed, M. G.; Gowrisanker, S.; Servello, J.; Stefan, M. C. Synthesis of Di-block Copolymers Containing Regioregular Poly(3-hexylthiophene) and Poly(tetrahydrofuran) by a Combination of Grignard Metathesis and Cationic Polymerizations. *Macromol. Chem. Phys.* **2009**, *210*, 2007−2014.

(21) Alemseghed, M. G.; Servello, J.; Hundt, N.; Sista, P.; Biewer, M. C.; Stefan, M. C. Amphiphilic Block Copolymers Containing Regioregular Poly(3-hexylthiophene) and Poly(2-ethyl-2-oxazoline). *Macromol. Chem. Phys.* **2010**, *211*, 1291−1297.

(22) Nguyen, H. Q.; Bhatt, M. P.; Rainbolt, E. A.; Stefan, M. C. Synthesis and characterization of a polyisoprene-b-polystyrene-b-poly(3-hexylthiophene) triblock copolymer. *Polym. Chem.* **2013**, *4*, 462.

(23) Palaniappan, K.; Hundt, N.; Sista, P.; Nguyen, H.; Hao, J.; Bhatt, M. P.; Han, Y.-Y.; Schmiedel, E. A.; Sheina, E. E.; Biewer, M. C.; Stefan, M. C. Block copolymer containing poly(3-hexylthiophene) and poly(4-vinylpyridine): Synthesis and its interaction with CdSe quantum dots for hybrid organic applications. *J. Polym. Sci., Part A: Polym. Chem.* **2011**, *49*, 1802−1808.

(24) Zhai, D.; Zhu, M.; Chen, S.; Yin, Y.; Shang, X.; Li, L.; Zhou, G.; Peng, J. Effect of Block Sequence in All-Conjugated Triblock Copoly(3-alkylthiophene)s on Control of the Crystallization and Field-Effect Mobility. *Macromolecules* **2020**, *53*, 5775−5786.

(25) Miyakoshi, R.; Yokoyama, A.; Yokozawa, T. Catalyst-Transfer Polycondensation. Mechanism of Ni-Catalyzed Chain-Growth Polymerization Leading to Well-Defined Poly(3-hexylthiophene). *J. Am. Chem. Soc.* **2005**, *127*, 17542−17547.

(26) Beryozkina, T.; Senkovskyy, V.; Kaul, E.; Kiriy, A. Kumada Catalyst-Transfer Polycondensation of Thiophene-Based Oligomers: Robustness of a Chain-Growth Mechanism. *Macromolecules* **2008**, *41*, 7817−7823.

(27) Hundt, N.; Hoang, Q.; Nguyen, H.; Sista, P.; Hao, J.; Servello, J.; Palaniappan, K.; Alemseghed, M.; Biewer, M. C.; Stefan, M. C. Synthesis and characterization of a block copolymer containing regioregular poly(3-hexylthiophene) and poly(γ-benzyl-L-glutamate). *Macromol. Rapid Commun.* **2011**, *32*, 302−308.

(28) Bhatt, M. P.; Du, J.; Rainbolt, E. A.; Pathiranage, T. M. S. K.; Huang, P.; Reuther, J. F.; Novak, B. M.; Biewer, M. C.; Stefan, M. C. A semiconducting liquid crystalline block copolymer containing regioregular poly(3-hexylthiophene) and nematic poly(n-hexyl isocyanate) and its application in bulk heterojunction solar cells. *J. Mater. Chem. A* **2014**, *2*, 16148−16156.

(29) Han, W.; He, M.; Byun, M.; Li, B.; Lin, Z. Large-Scale Hierarchically Structured Conjugated Polymer Assemblies with Enhanced Electrical Conductivity. *Angewandte Chemie International Edition* **2013**, *52*, 2564−2568.

(30) Yin, Y.; Chen, S.; Zhu, S.; Li, L.; Zhai, D.; Huang, D.; Peng, J. Tailoring Cocrystallization and Microphase Separation in Rod−Rod

https://doi.org/10.1021/acsomega.1c04176
ACS Omega 2021, 6, 27325−27334

Block Copolymers for Field-Effect Transistors. *Macromolecules* **2021**, *54*, 4571−4581.
(31) Wang, J.-S.; Matyjaszewski, K. Controlled/"living" radical polymerization. atom transfer radical polymerization in the presence of transition-metal complexes. *J. Am. Chem. Soc.* **1995**, *117*, 5614−5615.
(32) Matyjaszewski, K. Atom Transfer Radical Polymerization (ATRP): Current Status and Future Perspectives. *Macromolecules* **2012**, *45*, 4015−4039.
(33) Jeffries-El, M.; Sauvé, G.; McCullough, R. D. In-situ end-group functionalization of regioregular poly(3-alkylthiophene) using the Grignard metathesis polymerization method. *Adv. Mater.* **2004**, *16*, 1017−1019.
(34) Jeffries-El, M.; Sauvé, G.; McCullough, R. D. Facile Synthesis of End-Functionalized Regioregular Poly(3-alkylthiophene)s via Modified Grignard Metathesis Reaction. *Macromolecules* **2005**, *38*, 10346−10352.
(35) Iovu, M. C.; Sheina, E. E.; Gil, R. R.; McCullough, R. D. Experimental Evidence for the Quasi-"Living" Nature of the Grignard Metathesis Method for the Synthesis of Regioregular Poly(3-alkylthiophenes). *Macromolecules* **2005**, *38*, 8649−8656.
(36) Matyjaszewski, K.; Jakubowski, W.; Min, K.; Tang, W.; Huang, J.; Braunecker, W. A.; Tsarevsky, N. V. Diminishing catalyst concentration in atom transfer radical polymerization with reducing agents. *Proc. Natl. Acad. Sci.* **2006**, *103*, 15309−15314.
(37) Kim, J.-H.; Kim, H. U.; Kang, I.-N.; Lee, S. K.; Moon, S.-J.; Shin, W. S.; Hwang, D.-H. Incorporation of Pyrene Units to Improve Hole Mobility in Conjugated Polymers for Organic Solar Cells. *Macromolecules* **2012**, *45*, 8628−8638.
(38) Gong, Y.; Zhan, X.; Li, Q.; Li, Z. Progress of pyrene-based organic semiconductor in organic field effect transistors. *Sci China Chem.* **2016**, *59*, 1623−1631.
(39) Feng, X.; Hu, J.-Y.; Redshaw, C.; Yamato, T. Functionalization of Pyrene To Prepare Luminescent Materials—Typical Examples of Synthetic Methodology. *Chem. − Eur. J.* **2016**, *22*, 11898−11916.
(40) Zöphel, L.; Beckmann, D.; Enkelmann, V.; Chercka, D.; Rieger, R.; Müllen, K. Asymmetric pyrene derivatives for organic field-effect transistors. *Chem. Commun.* **2011**, *47*, 6960−6962.
(41) Shu, C.; Han, C.; Yang, X.; Zhang, C.; Chen, Y.; Ren, S.; Wang, F.; Huang, F.; Jiang, J.-X. Boosting the Photocatalytic Hydrogen Evolution Activity for D−π−A Conjugated Microporous Polymers by Statistical Copolymerization. *Adv. Mater.* **2021**, *33*, 2008498.
(42) Kim, A.; Lee, D. H.; Um, H. A.; Shin, J.; Cho, M. J.; Choi, D. H. Tunable light harvesting properties of a highly crystalline alternating terpolymer for high-performing solar cells. *Polym. Chem.* **2015**, *6*, 5478−5486.
(43) Yang, D. S.; Kim, K. H.; Cho, M. J.; Jin, J.-I.; Choi, D. H. Donor−acceptor alternating π-conjugated polymers containing Di(thiophen-2-yl)pyrene and 2,5-Bis(2-octyldodecyl)pyrrolo[3,4-c]-pyrrole-1,4(2H,5H)-dione for organic thin-film transistors. *J. Polym. Sci., Part A: Polym. Chem.* **2013**, *51*, 1457−1467.
(44) Kim, J.-H.; Lee, S.; Kang, I.-N.; Park, M.-J.; Hwang, D.-H. Photovoltaic devices using semiconducting polymers containing head-to-tail-structured bithiophene, pyrene, and benzothiadiazole derivatives. *J. Polym. Sci., Part A: Polym. Chem.* **2012**, *50*, 3415−3424.
(45) Wang, N.; Bao, X.; Yan, Y.; Ouyang, D.; Sun, M.; Roy, V. A. L.; Lee, C. S.; Yang, R. Synthesis and photovoltaic properties of conjugated D−A copolymers based on thienyl substituted pyrene and diketopyrrolopyrrole for polymer solar cells. *J. Polym. Sci., Part A: Polym. Chem.* **2014**, *52*, 3198−3204.
(46) Ndao, M.; Lefort, R.; Cerclier, C. V.; Busselez, R.; Morineau, D.; Frick, B.; Ollivier, J.; Kityk, A. V.; Huber, P. Molecular dynamics of pyrene based discotic liquid crystals confined in nanopores probed by incoherent quasielastic neutron scattering. *RSC Adv.* **2014**, *4*, 59358−59369.
(47) Gan, K. P.; Yoshio, M.; Kato, T. Columnar liquid-crystalline assemblies of X-shaped pyrene-oligothiophene conjugates: photoconductivities and mechanochromic functions. *J. Mater. Chem. C* **2016**, *4*, 5073−5080.
(48) Chen, L.; Peng, S.; Chen, Y. Cooperative Assembly of Pyrene-Functionalized Donor/Acceptor Blend for Ordered Nanomorphology by Intermolecular Noncovalent π−π Interactions. *ACS Appl. Mater. Interfaces* **2014**, *6*, 8115−8123.
(49) Pathiranage, T. M. S. K.; Kim, M.; Nguyen, H. Q.; Washington, K. E.; Biewer, M. C.; Stefan, M. C. Enhancing Long-Range Ordering of P3HT by Incorporating Thermotropic Biphenyl Mesogens via ATRP. *Macromolecules* **2016**, *49*, 6846−6857.
(50) Pathiranage, T. M. S. K.; Magurudeniya, H. D.; Bhatt, M. P.; Rainbolt, E. A.; Biewer, M. C.; Stefan, M. C. Synthesis and characterization of side-chain thermotropic liquid crystalline copolymers containing regioregular poly(3-hexylthiophene). *Polymer* **2015**, *72*, 317−326.
(51) Kline, R. J.; McGehee, M. D.; Kadnikova, E. N.; Liu, J.; Frechet, J. E. M. J.; Toney, M. F. Dependence of Regioregular Poly(3-hexylthiophene) Film Morphology and Field-Effect Mobility on Molecular Weight. *Macromolecules* **2005**, *38*, 3312−3319.
(52) Han, D.; Tong, X.; Zhao, Y.; Zhao, Y. Block Copolymers Comprising π-Conjugated and Liquid Crystalline Subunits: Induction of Macroscopic Nanodomain Orientation. *Angew. Chem., Int. Ed.* **2010**, *49*, 9162−9165.
(53) Tong, X.; Han, D.; Fortin, D.; Zhao, Y. Highly Oriented Nanofibrils of Regioregular Poly(3-hexylthiophene) Formed via Block Copolymer Self-Assembly in Liquid Crystals. *Adv. Funct. Mater.* **2013**, *23*, 204−208.
(54) Yuan, K.; Chen, L.; Chen, Y. Photovoltaic performance enhancement of P3HT/PCBM solar cells driven by incorporation of conjugated liquid crystalline rod-coil block copolymers. *J. Mater. Chem. C* **2014**, *2*, 3835−3845.
(55) Bhatt, M. P.; Sista, P.; Hao, J.; Hundt, N.; Biewer, M. C.; Stefan, M. C. Electronic Properties-Morphology Correlation of a Rod−Rod Semiconducting Liquid Crystalline Block Copolymer Containing Poly(3-hexylthiophene). *Langmuir* **2012**, *28*, 12762−12770.

https://doi.org/10.1021/acsomega.1c04176
ACS Omega 2021, 6, 27325−27334